A Small-Size Foreign Metal Objects Detection Based on Rectangular-Coil Array for DWPT Systems

Xiaodong Yang, Yuzhao Ouyang, Kaiwen Chen, *Member, IEEE*, Norbert Cheung, *Senior Member, IEEE*, and Jianfei Pan, *Member, IEEE*

***Abstract*— This article proposes a new detection method for foreign metal objects (FMOs) based on a new detection array. Compared with traditional FMO detection (FMOD), the proposed method can detect smaller FMOs without any external sensors. The nature of the method is to decouple the receiving (Rx) coil that has similar feedback characteristics to small-size FMOs. Hence, the cost of FMOD system is reduced in the actual implementation. Furthermore, this kind of FMOD does not require communication. So, it has high stability and can be easily realized. Finally, the experimental results prove that the proposed method has a high effectiveness for detecting small-size FMOs (able to detect FMOs up to 1.08 cm^2).**

***Index Terms*— Dynamic wireless power transfer (DWPT), foreign metal object detection (FMOD), inductive zone detection.**

NOMENCLATURE

$V_{\rm dc}$	DC source.
v_T	Output of the inverter.
L_T	Self-inductance of the Tx coil.
C_T	Compensated capacitor for the Tx.
R_T	Equivalent series resistance of L_T and C_T.
Z_T	Impedance of the Tx-side resonator.
i_T	Current of the Tx side.
L_A	Self-inductance of the sensing coil.
L_F	Self-inductance of the FMO.
R_F	Resistance of the FMO.
Z_F	Equivalent impedance of FMO.
v_A	Induced voltage of L_A.
M_{TA}	Mutual inductance between L_T and L_A.
M_{TF}	Mutual inductance between L_T and L_F.
M_{TR}	Mutual inductance between L_T and L_R.
M_{RA}	Mutual inductance between Rx and L_A.
M_{FA}	Mutual inductance between FMO and L_A.
M_{FR}	Mutual inductance between FMO and Rx.
L_R	Self-inductance of the Rx coil.
C_R	Compensated capacitor for the Rx.
R_R	Equivalent series resistance of L_R and C_R.
Z_R	Impedance of the Rx-side resonator.
v_R	Output voltage of Rx-side resonator.
R_{eq}	Equivalent resistance of the load.
i_R	Current of the receiving side.
φ	Symbol of detection criteria.
φ_{no}	The value of φ of the normal mode.
φ_{FO}	The value of φ when FMO on the platform.
φ_{Rx_min}	The value of φ when receiver on the platform.
φ_{Rx}	The value of φ when the M_{TR} is maximum.
i_{T_no}	The value of i_T when platform have nothing.
i_{T_FO}	The value of i_T when FMO on the platform.
i_{T_Rx}	The value of i_T when Rx on the platform.
L_T'	Self-inductance of the L_T in the normal mode with inductive zone detection method.
L_T''	Self-inductance of the L_T in the FMO mode with inductive zone detection method.

Manuscript received 8 December 2023; revised 22 February 2024; accepted 28 February 2024. Date of publication 25 March 2024; date of current version 5 April 2024. This work was supported in part by the National Natural Science Foundation of China under Grant 52277060 and in part by the Shenzhen Science and Technology Program under Grant JCYJ20220818100000001 and Grant SGDX20230116110009018. The Associate Editor coordinating the review process was Dr. Hamed Hamzehbahmani. *(Corresponding author: Jianfei Pan.)*

The authors are with the College of Mechatronics and Control Engineering, Shenzhen University, Shenzhen 518061, China (e-mail: pjf@szu.edu.cn).

Digital Object Identifier 10.1109/TIM.2024.3381265

I. INTRODUCTION

IN RECENT years, dynamic wireless power transfer (DWPT) technology has been getting more attention because it does not require the receiving (Rx) coils to locate in a fixed position [1], [2]. DWPT has broadened the horizons of wireless power transfer (WPT). DWPT has been widely used in many industrial applications, such as automated guided vehicle (AGV). However, DWPT has a unique safety issue during the working process. The operation of DWPT requires the generation of a high-frequency alternating magnetic field, which lead to the generation of heat on the foreign metal objects (FMOs), will inevitably result in fires and cause substantial damage to the working environment. Therefore, it is the imperative to detect the presence of FMOs on the DWPT working platform, and WPT can be mainly divided into electromagnetic radiation WPT (ERWPT) [3], [4], [5], capacitive WPT (CWPT) [6], [7], and inductive WPT (IWPT) [8], [9], [10], but IWPT has attracted more researchers' interest due to its relatively long transfer distance and high transmission efficiency [11], [12]. It has been applied in WPT for electric vehicles [13], unmanned ariel vehicles [14], and AGVs [2], and in dynamic IWPT system, the magnetic field

between the transmitting (Txs) and Rxs is extremely strong, so that the foreign metal causes the fire by eddy currents easily. So, it is necessary to detect FMOSs on the platform in dynamic IWPT. Prior researchers have made considerable efforts focus on FMOD [15], [16], [17], [18]. However, a persistent challenge exists due to the similarities in feedback characteristics between the small-size FMOs and the Rx coils because the sensing coil usually cannot distinguish them.

In response to the issue of small-size FMOs, there are several methods on the FOMD in DWPT. It can be roughly be divided into three types, including system parameter estimation (SPD) [18], [19], [20], [21], [22], detection based on external sensors (ESD) [23], [24], [25], [26], [27], and detection based on detection coils (SCD) [30], [31], [32], [33], [34].

SPD method evaluates the parameter changes of an inductance WPT (IWPT) system to determine the existence of FMOs. The detection metrics includes quality factor [18], resonant frequency [19], power loss [20], current [21], coupling coefficient [22], and so on. These methods are easy to implement, and the cost is relatively low. However, it is difficult to detect small-size FMOs by these methods, and they are only confined to the IWPT systems, where the coil positions are fixed. ESD uses external sensing equipment, such as thermal cameras [23], magnetic sensors [24], radar sensors [25], lidar devices [26], and ultrasonic transducers [27], to detect the existence of an FMO. These methods can detect FMOs with high accuracy. However, the sensing devices are difficult to integrate into IWPT system, and communication unit between them is needed, which makes the system very complex and expensive.

SCD methods are more popular compared to the SPD and ESD methods [28], [29]. A sensing coil or coil array is placed on the Tx coils to detect the FMOs. An FMO in the IWPT system can change the magnetic field around it. Therefore, measuring the induced voltage variation on additional sensing coils can be applied to detect the FMO effectively. In [30], an FOD method based on symmetrical coil sets is proposed, but blind zones of detection exist at the center region of the coil sets. In [31], the self-inductance changes of the sensing coils are evaluated by a parallel resonant circuit. The proposed method can detect small-size FMODs without any blind zones. However, the cost of this method is high due to the complicated noise filter design and the requirement of multilayer sensing coil sets. In [32], by introducing a two-layer sensing coil set, the number of blind zones can be reduced, but the proposed method also increases the cost significantly. According to the abovementioned articles, an FMOD method for the dynamic IWPT system without the detection blind zones is needed to be proposed. This method should be able to detect FMOs in any size, and the system should be simple structure and low cost. Besides, the proposed method should be able to distinguish FMOs from the Rxs.

This article proposes a better scheme that is required to eliminate the above shortcomings. To this end, this article proposes a free-communication FMOD for series–series compensation DWPT system with a new detection array. Through mathematical modeling and analysis of the circuit, the impedance generated by FMOs and the Rx side is compared and analyzed, so that it can distinguish between the Rx side and FMOs. The main contributions for this novel method can be summarized as follows.

1) *Detectability of Full-Size FMOs:* By decoupling the impedance produced by small-size FMOs and the Rx side, effectively distinguishing the presence of FMOs on the work platform.
2) *New Detection Array:* By using a detection array composed of rectangular coils, it eliminates the detection gap caused by the circular coil structure.
3) *Low Implementation Cost*: No image sensors or communication units are involved. Therefore, the system is simple with low cost and easy to realize.

II. System Modeling and Concept of the Sensing Coil-Based FMOD Scheme

A. Modeling of the Proposed Multi-Txs Dynamic WPT System for AGVs

The overall configuration of the proposed coil array-based dynamic WPT system for AGVs is illustrated in Fig. 1(a). The working platform of AGVs is covered with ferrites, which helps to enhance the coupling performance and to decrease the leakage inductance. An aluminum shield is placed under the ferrites, which is utilized to avoid electromagnetic interference to the surroundings. A rectangular Tx coil array is placed on the ferrites for energizing adequate EMF for power transmission. Besides, an open-circuit sensing coil array is covered on the Tx array for metal object detection. The rectangular shape ensures that the Tx coils and the Rx coils can fully cover the whole of the working platform, and there will be no blind spot of power transmission detection. This system can deliver energy to the AGVs, which are moving on the platform. The basic component of the system is depicted in Fig. 1(b).

The circuit model of the component is shown in Fig. 2. The Tx coil (i.e., L_T) is driven by a full-bridge inverter (i.e., S_1S_4), where V_{dc} is the input direct current (dc) voltage. v_T and i_T represent the input alternating current (ac) voltage and current, respectively. C_T is the compensated capacitor for the Tx, and R_T is the equivalent series resistance (ESR) of L_T and C_T. Z_T represents the impedance of the Tx-side resonator, which can be expressed as follows:

$$Z_T = R_T + j\left(\omega L_T - \frac{1}{\omega C_T}\right) \tag{1}$$

where $\omega = 2\pi f$ is the angular frequency, and f is the switching frequency of the full-bridge inverter. The inverter is controlled by a digital signal processor (DSP). The Rx resonator consists of an inductive coil L_R and its compensated capacitor C_R, and the ESR in the Rx resonator is expressed as R_R. The mutual inductance between the Tx and Rx is represented by M_{TR}. v_R and i_R are the resonator voltage and current of the Rx, respectively. The diode rectifier (i.e., D_1–D_4) feeds the AGV loads (i.e., R_L) with dc output voltage and current (i.e., V_o and i_o). A regulator capacitor C_o is employed to filter the ac components. R_{eq} is the equivalent

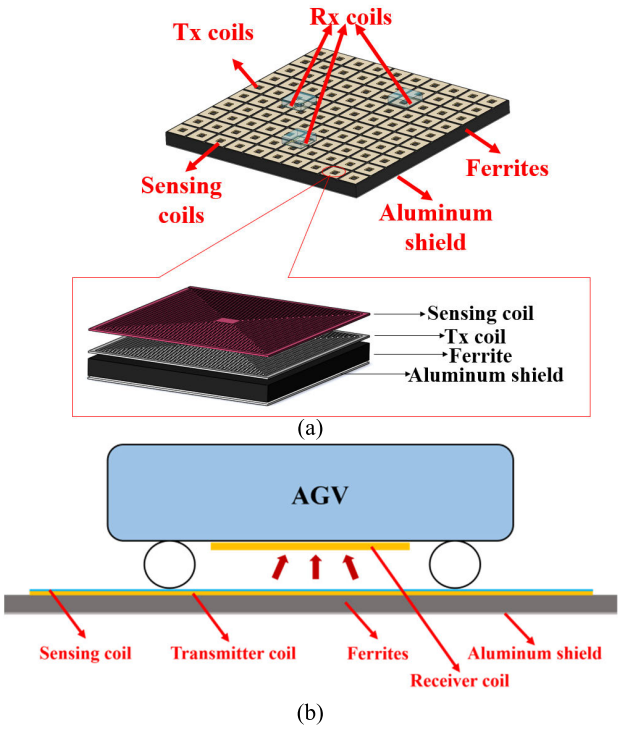

Fig. 1. (a) Configuration of the proposed dynamic WPT system for AGVs. (b) Basic unit of the WPT system.

resistance of the load, and Z_R is the impedance of the Rx side, which can be expressed as

$$Z_R = R_R + R_{\text{eq}} + j\left(\omega L_R - \frac{1}{\omega C_R}\right). \tag{2}$$

The open-circuit auxiliary sensing coil is utilized to detect the potential metal objects in the IWPT system. The inductance of the sensing coil is represented by L_A, and v_A is its induced voltage. M_{TA} is the mutual inductance between L_T and L_A. Generally, a metal object in a WPT system can be replaced by an equivalent inductor with a series resistance [35]. The equivalent inductance and resistance of the eddy winding in the metal object are represented by L_F and R_F, respectively. M_{TF} is the mutual inductance between L_T and L_F.

B. Implementation of FMOD Using Sensing Coil Array

Three models, including the normal model, the FMO model, and the Rx model, are established to distinguish between the different situations, as demonstrated in Fig. 3. The normal model includes Tx coils and sensing coils, as depicted in Fig. 3(a). In this case, there is no metal object or Rx coil on the platform. According to the Kirchhoff laws, which is commonly applied in modeling WPT system [37], [38], [39], the induced voltage in the sensing coil can be expressed as follows:

$$v_A = j\omega M_{TA} i_T. \tag{3}$$

Thus, we have

$$\varphi_{\text{no}} = \left(\frac{v_A}{i_T}\right)_{\text{no}} = j\omega M_{TA} \tag{4}$$

where the subscript "no" represents "normal," and $\varphi = (v_A)/(i_T)$ is used as the detection criterion.

When there is an FMO on the platform, as shown in Fig. 3(b), the sensing coil is also induced by the metal object. M_{FA} represents the mutual inductance between L_A and L_F. In this case, according to the Kirchhoff laws

$$v_A = j\omega M_{TA} i_T + j\omega M_{FA} i_F \tag{5}$$

$$j\omega M_{TF} i_T = Z_F i_F \tag{6}$$

where Z_F represents the equivalent impedance of the metal object

$$Z_F = R_F + j\omega L_F. \tag{7}$$

By combining (5) and (6), we have

$$\varphi_{\text{FO}} = j\omega M_{TA} - \frac{\omega^2 M_{FA} M_{TF}}{Z_F}. \tag{8}$$

The influence of FMOs on the Tx side is measured in the experimental practice, and the analysis is shown in the Appendix. The experimental results show that a metal object on the platform reduces the self-inductance of the Tx and the sensing coil and the mutual inductance between them. Therefore, the value of M_{TA} in the FMO model is always lower than the normal model, and the value of φ_{FO} is thus lower than φ_{no}

$$\varphi_{\text{FO}} = j\omega(M_{TA} - \Delta M_{\text{fo}}) - \frac{\omega^2 M_{FA} M_{TF}}{Z_F} = \varphi_{\text{no}} - \Delta\varphi_{\text{fo}}. \tag{9}$$

When there is a Rx coil, as demonstrated in Fig. 3(c), the sensing coil is coupled with both L_T and L_R. M_{RA} represents the mutual inductance between L_A and L_R. In this case, the induced voltage can be expressed as follows:

$$v_A = j\omega M_{TA} i_T + j\omega M_{RA} i_R \tag{10}$$

and in the Rx side, we have

$$j\omega M_{TR} i_T = Z_R i_R. \tag{11}$$

By combining (10) and (11), (12) is derived

$$\varphi_{\text{Rx}} = j\omega M_{TA} - \frac{\omega^2 M_{RA} M_{TR}}{Z_R} = \varphi_{\text{no}} - \Delta\varphi_{\text{rx}}. \tag{12}$$

M_{RA} and M_{TR} increase with the alignment of the Rx due to stronger coupling. The increment of M_{RA} and M_{TR} causes a reduction of φ

$$\varphi_{Rx} - \Delta\varphi = j\omega M_{TA} - \frac{\omega^2 (M_{RA} + \Delta M_1)(M_{TR} + \Delta M_2)}{Z_R}. \tag{13}$$

When the Rx coil moves to the optimum coupling position with the Tx coil, φ_{Rx} reaches its minimum value

$$\varphi_{\text{Rx\_min}} = j\omega M_{TA} - \frac{\omega^2 M_{\text{RA\_max}} M_{\text{TR\_max}}}{Z_R}. \tag{14}$$

When both the Rx end and FMO appear on the work platform, based on previous analysis, the presence of FMO will make $\varphi_{\text{FO}} < \varphi_{\text{Rx\_min}}$. Therefore, when modeling FMO,

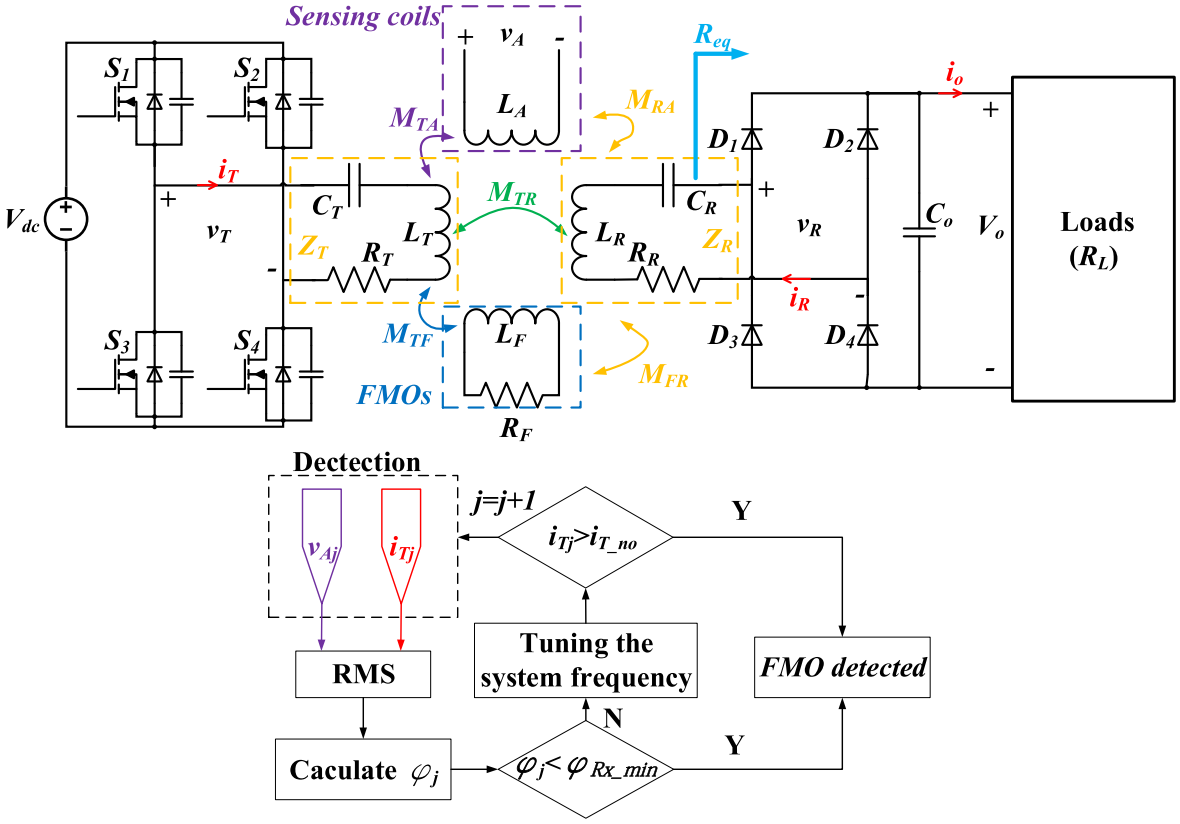

Fig. 2. Circuit model of the coil array-based DWPT.

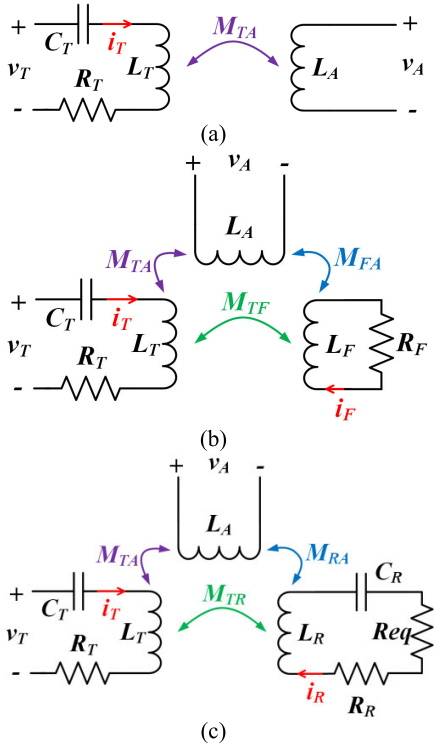

Fig. 3. Models under different conditions. (a) Normal model. (b) FMO model. (c) Rx model.

the mutual inductance between FMO and the Rx-side M_{FR} can be ignored. The influence of FMO on φ is stronger than that of Rx, and φ_{FO} is always lower than φ_{Rx_min} when there is FMO in the IWPT system. Therefore, by measuring φ, FMO in the IWPT system can be detected.

III. Inductive Zone Detection and Implementation of the FMOD Scheme

A. Feasibility Analysis of the Inductive Zone Detection

If the size of an FMO is too small, φ_{FO} is similar to φ_{Rx}, and φ is no longer suitable to be a criterion of detection. Therefore, an advanced scheme must be utilized for more precise detection. In advanced detection, the system is needed to work in the inductive zone.

In the normal model, when the system frequency is set higher than the Tx-side resonant frequency, according to the Ohm law

$$\frac{v_T}{i_{T\_no}} = R_T + j\left(\omega_d L_T - \frac{1}{\omega_d C_T}\right) = R_T + j\omega_d L_T' \tag{15}$$

where ω_d is the detecting frequency ($\omega_d > \omega_t$, and ω_t is the resonant frequency of Tx side), $j\omega_d L_T'$ is the equivalent reactance of L_T and C_T in the normal model when the system frequency is equal to ω_d, and i_{T_no} is the input ac current in this case. In this case, the system works in the inductive zone.

In the FMO model, according to the Kirchhoff law, the input ac voltage can be expressed as follows:

$$v_T = Z_T i_T - j\omega M_{TF} i_F. \tag{16}$$

Normally, the resistance of a metal object is pretty low, and therefore, the resonant current of the metal object can be

expressed as follows:

$$i_F = \frac{j\omega M_{TF} i_T}{R_F + j\omega L_F} \approx \frac{M_{TF} i_T}{L_F}. \tag{17}$$

When the system frequency ω is equal to ω_d, by combining (16) and (17), we have

$$\frac{v_T}{i_{T\_FO}} = R_T + j\left(\omega_d L_T'' - \frac{\omega M_{TF}^2}{L_F}\right) \tag{18}$$

where $j\omega_d L_T''$ is the equivalent reactance of L_T and C_T in the FMO model when the system frequency is equal to ω_d.

According to the analysis in the Appendix, L_T'' is always lower than L_T'. Therefore, when the system frequency is higher than ω_t, an FMO can lower the equivalent input impedance of the Tx side. Since v_T is fixed, we have

$$i_{T\_\mathrm{FO}} > i_{T\_\mathrm{no}}. \tag{19}$$

In the Rx model, according to the Kirchhoff law, we have

$$v_T = Z_T i_T - j\omega M_{TR} i_R. \tag{20}$$

By combining (11) and (20), we have

$$\frac{v_T}{i_{T\_\mathrm{Rx}}} = Z_T + \frac{\omega^2 M_{TR}^2}{Z_R}. \tag{21}$$

It is obvious that the equivalent input impedance of the Tx side increases when Rx coil is existed, and the value of i_T in this case is thus lower than the normal case

$$i_{T\_\mathrm{Rx}} < i_{T\_\mathrm{no}} < i_{T\_\mathrm{FO}}. \tag{22}$$

Therefore, by measuring the value of i_T, the system is able to detect metal objects even with a small size and distinguish them from Rx coils.

B. Implementation of the FMOD Scheme

By measuring the value of φ and i_T, the system is able to detect any FMOs in the IWPT system. After the system is built, the value of $\varphi_{\mathrm{Rx\_min}}$ and i_{T_no} can be measured. Since the parameters of each Tx coil are the same, they share the same value of $\varphi_{\mathrm{Rx\_min}}$ and i_{T_no}. In the proposed multi-Tx system, each Tx coil is marked from 1 to n, respectively. The flowchart of the FMOD scheme is described in Fig. 4. When the detecting process starts, the first Tx coil is activated, and the induced voltage of its sensing coil v_{A1} and its winding current i_{T1} is measured. By calculating φ_1 from v_{A1} and i_{T1} and comparing it with $\varphi_{\mathrm{Rx\_min}}$, the following scenarios are reached. If φ_1 is lower than $\varphi_{\mathrm{Rx\_min}}$, this indicates that Tx 1 is covered with FMOs, and this coil will be turned off immediately to protect the IWPT system. If φ_1 is equal to or higher than $\varphi_{\mathrm{Rx\_min}}$, the inductive zone detection is needed to carry out.

To realize the inductive zone detection, the system frequency is tuned to the inductive zone frequency, and the value of i_{T1} is measured in this case. If i_{T1} is higher than i_{T_no}, there are FMOs exist, and Tx 1 will be turned off. If i_{T1} is equal to or lower than i_{T_no}, there is no metal object over Tx 1, and this coil will be energized to delivery power to the Rx coils. The detecting criterion of FMOs is depicted in Fig. 5. After

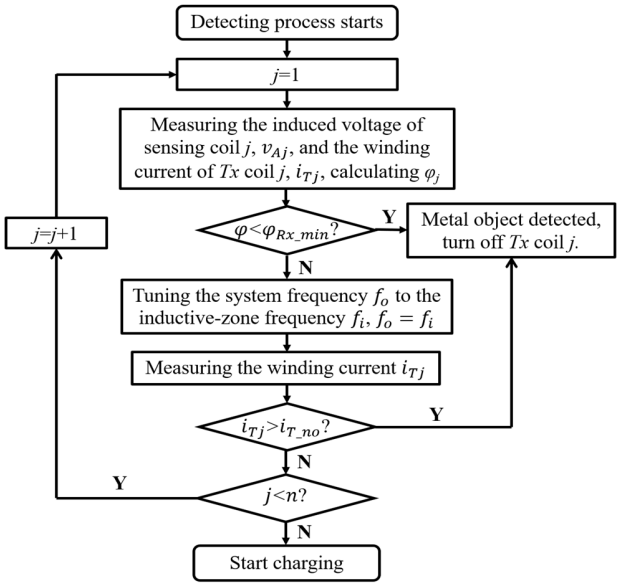

Fig. 4. Flowchart of the FMOD scheme.

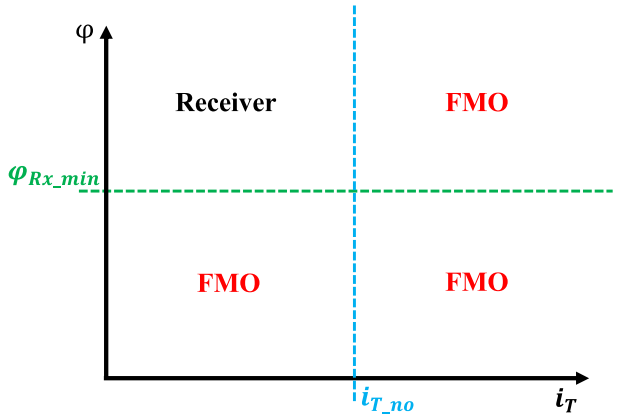

Fig. 5. Detecting criterion of foreign metal objects.

one Tx block is detected, the system starts to detect the next one, until all Tx coils are scanned.

There are two detection methods, which are aimed at enhancing system efficiency. This is because when detecting small FMOs, it is necessary to adjust the work frequency. It can cause the system to deviate from its resonant frequency, thereby reducing the transmission efficiency of DWPT system. However, when detecting medium or large FMOs, it does not impact the transmission efficiency. When the FMOs detected with (14), the controller sends a signal, prompting the system to stop working, requiring manual intervention to eliminate potential hazards. If FMOs cannot be detected by $\varphi_{\mathrm{Rx\_min}}$, the controller adjusts the work frequency and changes the criteria with (22), ensuring whether FMOs are present on the platform.

IV. Experimental Verification

The experimental platform of this article is demonstrated in Fig. 6(a). The system is powered by SIGLENT SPD3303X programmable dc power supply. The Tx coil array contains nine rectangular coils with 18.5 turns, and the side length of each coil is 100 mm, as shown in Fig. 6(c). The Rx coil has

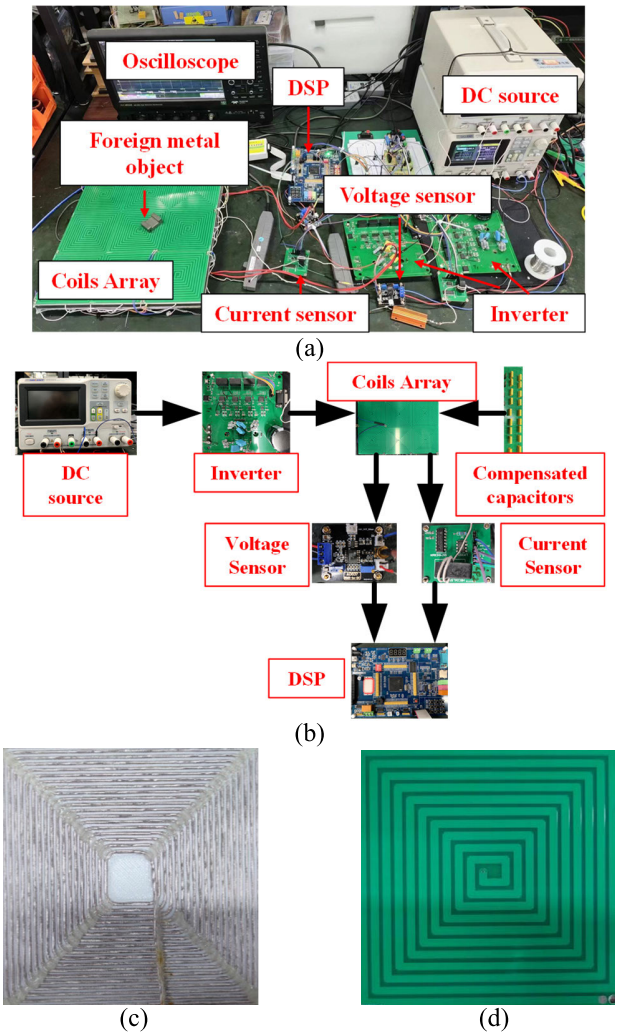

Fig. 6. (a) Experimental platform. (b) Schematic. (c) Tx and Rx coils. (d) Sensing coil.

the same size as the Tx coils. The size of ferrite in the Tx side is 300 × 300 × 10 mm, and the aluminum shield is 300 × 300 × 2 mm. The auxiliary sensing coil array contains nine rectangular coils with 20 turns, and the side length of each coil is also 100 mm. The sensing coils are placed on printed circuit boards (PCBs), as depicted in Fig. 6(d). The DSP for the Tx-side control and FMOD is TMS320F28335. The MOSFETs of the inverter are IRF740. The waveforms are captured by TELEDYNE LECROY HDO4024A oscilloscope. The parameters of the components, such as L_T, C_T, and R_T, are measured by TONGHUI TH2829AX LCR Meter under the operating frequency of 100 kHz and measuring voltage of 1 V.

The key parameters are listed in Table I.

A. Verification of FMOD Method Using Sensing Coils

This experiment was conducted to verify the feasibility of the proposed sensing coils. In the normal case, with 2 V of input voltage and 100 kHz of switching frequency, the values of v_A and i_T were measured, and the value of φ_{no} was calculated according to the measured results. In the experimental platform, the value of φ_{no} is 14.58, as depicted in Fig. 7. The scale of the oscilloscope is 10 μs/div in time, 10 V/div in voltage, and 2 A/div in current.

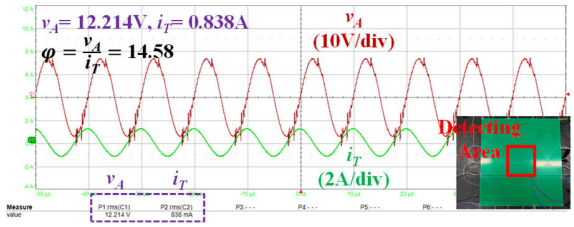

Fig. 7. Detecting result of the normal case.

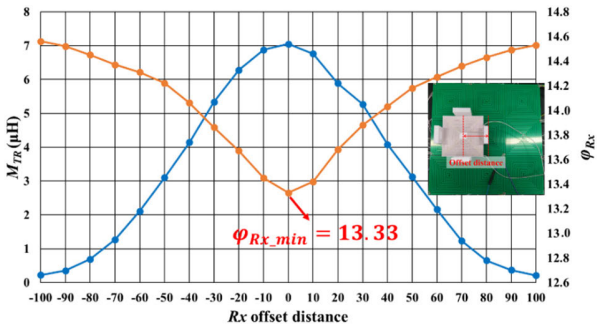

Fig. 8. Relationship of φ_{Rx} and M_{TR} with various Rx lateral offset distances.

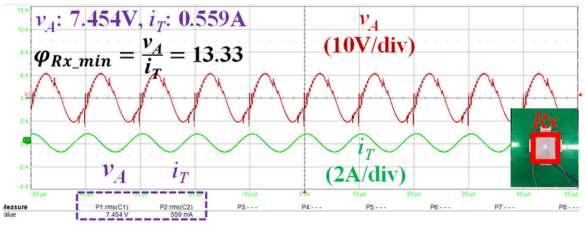

Fig. 9. Value of φ_{Rx_min} of the experimental platform.

To validate the effectiveness of our sensing coils in detecting FMOs, we conducted a series of experiments to distinguish the influence of Rx coil changes caused by FMOs from other factors. Using the FMOD method, outlined in (14), we first identified the minimum threshold value for the Rx coil φ_{Rx_min} that would indicate the presence of FMOs.

The experiment involved positioning the Rx coil at varying lateral offsets from the Tx coil to measure its magnetic coupling coefficient M_{TR} and the corresponding phase shift φ_{Rx}. Fig. 8 illustrates the relationship between φ_{Rx} and M_{TR} as the Rx coil is laterally displaced. From our measurements, we determined the threshold φ_{Rx_min} to be 13.33, as demonstrated in Fig. 9. This value serves as the criterion for FMO detection using the FMOD method.

We proceeded to test various metal objects, as listed in Table I, which included a nickel coin, a copper pillar, an aluminum block, an iron blade, and an aluminum sheet. Each metal object was placed onto the platform individually, and the resulting value of φ was calculated by controller. The waveforms generated for the different scenarios are presented in Fig. 10(a)–(e), and the result of the detection is shown in Fig. 12(a).

Analyzing the results, we observed that for case3 through case5, the values of φ were below the threshold φ_{Rx_min}.

TABLE I
KEY PARAMETERS (MEASUREMENT CONDITION: 100 KHZ, 1 V)

	Symbol	Value	Symbol	Value	Symbol	Value
Tx-side	L_{T1}	36.6 uH	C_{T1}	68.9 nF	R_{T1}	0.25 Ω
	L_{T2}	36 μH	C_{T2}	69.3 nF	R_{T2}	0.32 Ω
	L_{T3}	35.8 μH	C_{T3}	69.2 nF	R_{T3}	0.29 Ω
	L_{T4}	36.3 μH	C_{T4}	67.8 nF	R_{T4}	0.25 Ω
	L_{T5}	37.4 μH	C_{T5}	68.3 nF	R_{T5}	0.32 Ω
	L_{T6}	36.1 μH	C_{T6}	68.5 nF	R_{T6}	0.19 Ω
	L_{T7}	37.2 μH	C_{T7}	69.4 nF	R_{T7}	0.31 Ω
	L_{T8}	35.6 μH	C_{T8}	67.9 nF	R_{T8}	0.28 Ω
	L_{T9}	36.9 μH	C_{T9}	68.8 nF	R_{T9}	0.29 Ω
	Air gap	30 mm	C_o	200 μF	R_L	10 Ω
Rx	L_{R1}	20.9 μH	C_{R1}	119.3 nF	R_{R1}	0.26 Ω

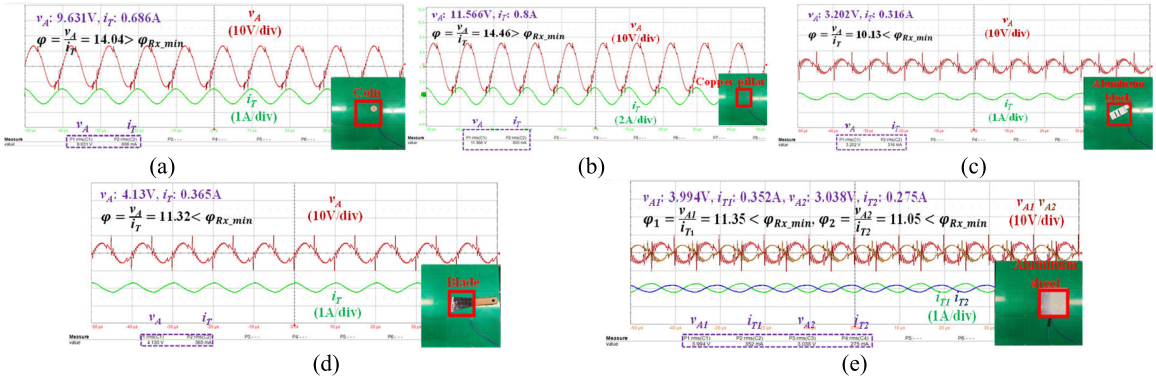

Fig. 10. Waveforms of the detecting results of different FMOs. (a) Case 1: coin. (b) Case 2: copper pillar. (c) Case 3: aluminum block. (d) Case 4: iron blade. (e) Case 5: aluminum sheet.

TABLE II
METAL OBJECTS AND THE DETECTED RESULTS

Object	Size(cm^2)	Material	FMOD by sensing coils	FMOD by inductive zone detection
Copper pillar	1.08	Copper	Not detected	Detected
Coin	4	Nickel	Not detected	Detected
Aluminum block	19	Aluminum	Detected	Detected
Blade	28.08	Iron	Detected	Detected
Aluminum sheet	100	Aluminum	Detected	Detected

This indicates that our sensing coils can successfully detect medium- or large-sized FMOs. However, cases 1 and 2 showed φ higher than $\varphi_{\text{Rx\_min}}$, suggesting that smaller sized FMOs, such as a nickel coin or a copper pillar, may not be detected under the current setup.

In conclusion, while this system is effective at identifying larger FMOs, additional refining of the inductive zone detection approach is required to improve the sensitivity toward smaller objects.

B. Verification of the Inductive Zone Detection Method

In previous experiments, we encountered a limitation, where small FMOs were undetectable by our sensing coils within the IWPT system. To address this, we explored an inductive zone detection method designed to identify small FMOs that the sensing coils might overlook.

The experiment aimed to test the effectiveness of this method by adjusting the system's operating frequency to be slightly higher than the resonant frequency of the Tx side, thus ensuring operation in the inductive zone. Specifically, we set the detection frequency to 105 kHz.

We compared the waveforms under different conditions, which are depicted in Fig. 11, and the detection results of FMOD method using sensing coil and the inductive zone detection method are shown in Fig. 12(a) and (b), respectively. Furthermore, we summarized the detection outcomes in Table II.

In a normal operating scenario without any FMOs, with an input voltage of 2 V, the reference current i_{T_no} in the Tx

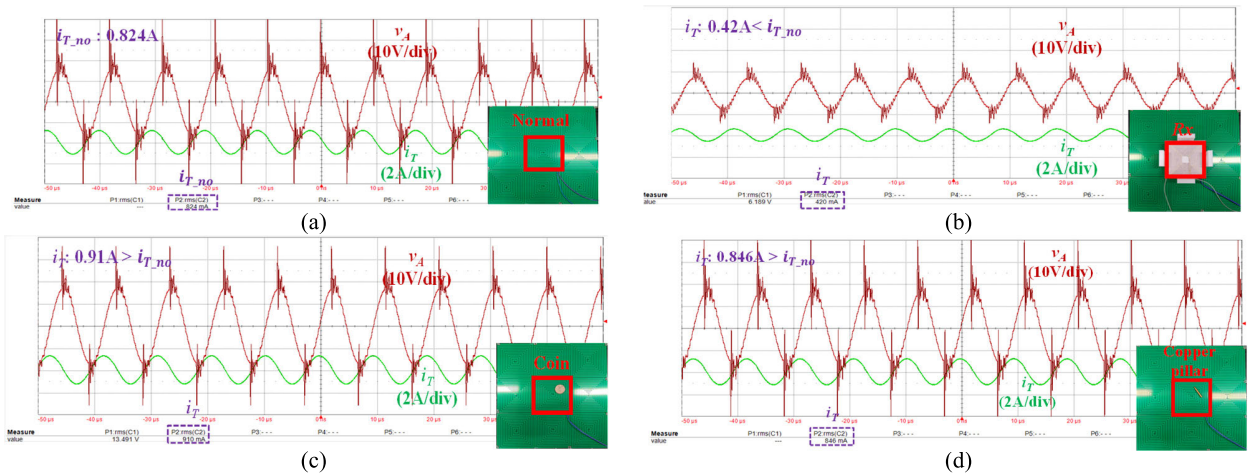

Fig. 11. Waveforms of the inductive zone detection. (a) Normal case. (b) Rx case. (c) Case 1: coin. (d) Case 2: copper pillar.

TABLE III
COMPARISON STUDY BETWEEN RELATED REFERENCES AND THE PROPOSED SYSTEM

Reference	Blind area	Coupling Condition	External Sensor	Communication	Distinguish between FMO and Receiver	The smallest detectable FMO
[24]	YES	Dynamic	NO	NO	Not Given	Coin
[28]	NO	Dynamic	Camera	YES	YES	/
[24]	Not Given	Dynamic	NO	NO	Not Given	Coin
[34]	YES	Static	NO	YES	NO	Coin
[35]	NO	Static	NO	NO	Not Given	Coin
This Work	NO	Dynamic	NO	NO	YES	Copper pillar (1.08 cm^2)

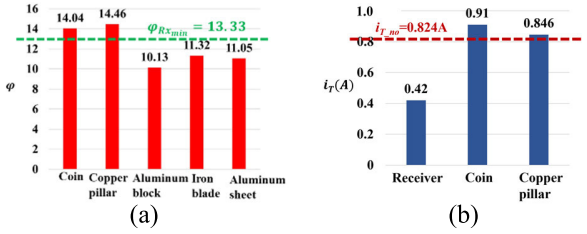

Fig. 12. (a) Detecting results of different FMOs. (b) Results of the inductive zone detection.

coil was measured at 0.824 A. When a Rx side was introduced, the measured current i_T dropped to 0.42 A, indicating the expected load behavior. However, in the presence of small FMOs (case1 and case2 from the prior experiment in Section IV-A), the measured currents i_T were 0.91 and 0.864 A, respectively. These values are notably higher than the reference current i_{T_no}. Based on the conclusions analyzed in Section III-A, we initially determine that when there is no Rx side and no FMO present on the work platform, the current $i_{T\_no} = 0.824$ A. When the system begins detection, the detected current $i_T = 0.42$ A is less than 0.824 A, and we determine that there is a Rx-side coil on the work platform rather than an FMO. When the detected current $i_T = 0.91$ A is greater than 0.824 A, we determine that there is an FMO on the work platform.

Thus, we conclude that the inductive zone detection method is effective in identifying small-sized FMOs and can differentiate them from the load represented by the Rx. The details of the detection results, including the variations in current measurements and their implications, are presented in Fig. 11. This method could significantly enhance the safety and functionality of IWPT systems by ensuring the detection of potentially disruptive small FMOs.

V. CONCLUSION AND DISCUSSION

A coil array-based FMOD method for AGVs dynamic IWPT system is presented in theory and experiment. A sensing coil array is utilized to detect FMOs of medium and big size, and an inductive zone detection method is proposed to detect further small-sized FMOs. The array structure and rectangular shape of coils ensure a detection range without any blind spots.

As shown in Table III, Jafari et al. [24] can effectively detect FMOs and even detect coins. However, due to the structure of the detection array, there are blind spots in the detection capability. Sonnenberg et al. [28] used a camera to address this issue, but this increases the implementation costs. Xiang et al. [34] also have a method that can effectively detect FMOs, but it requires communication, which can make the detection unstable. Compared with other related work in these years, the proposed system has the major advantage.

1) The proposed method has no blind area and there are no size restrictions for the FMO under detection. The experiment can detect copper pillars as small as 1.08 cm^2.

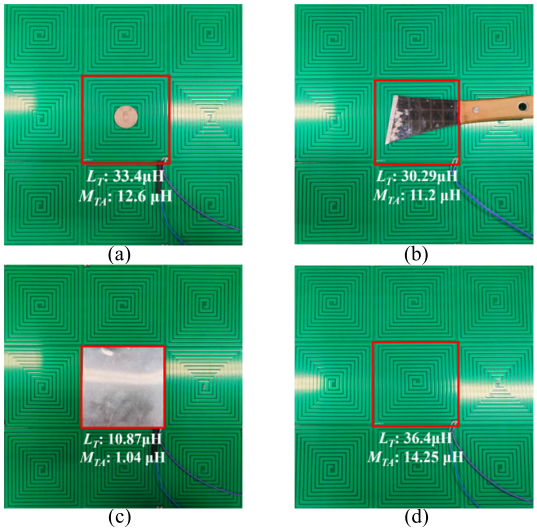

Fig. 13. (a) FMO of small size. (b) FMO of medium size. (c) FMO of big size. (d) Normal case.

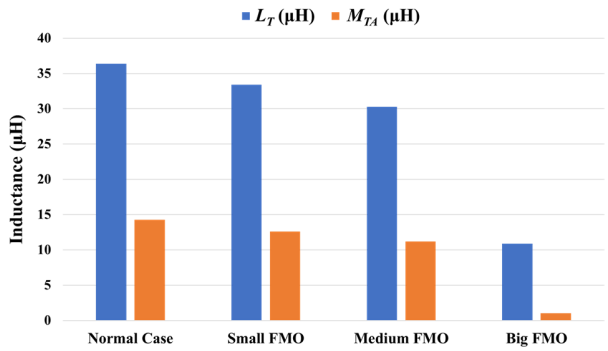

Fig. 14. Influence of FMOs on the Tx side.

2) The proposed method can distinguish metal objects from the Rxs; thus, it will not affect the normal operation of the system.

3) The proposed method requires only Tx-side measurements and does not require any image sensors or intercommunication units. Therefore, the system is simple, easy to realize, and the cost is low.

However, the detection method we proposed also has certain limitations and requires the determination of different detection criteria based on different system parameters in advance. Additionally, as the system operating time increases and system parameters change, this might affect the detection. Therefore, we need to explore more advanced and widely applicable FMO detection methods to address the existing issues.

APPENDIX

The self-inductance of the Tx coils and the mutual inductance between Txs and the sensing coils will lower when there is an FMO in the IWPT system. The influence of FMOs on the Tx side is verified by experiment. There are metal objects with kinds of size on the Txs separately, as depicted in Fig. 13(a)–(c). The normal case is also tested for comparation, as shown in Fig. 13(d). The results are demonstrated in Fig. 14. Experimental results show that an FMO in the IWPT system can lower the value of L_T and M_{TA}, and the influence is stronger with the increase of coverage area.

REFERENCES

[1] Y. Lin, Y. Xu, J. Zhu, X. Wang, L. Wang, and G. Hu, "MLATSO: A method for task scheduling optimization in multi-load AGVs-based systems," *Robot. Comput.-Integr. Manuf.*, vol. 79, Feb. 2023, Art. no. 102397.

[2] Z. Wang and Q. Zeng, "A branch-and-bound approach for AGV dispatching and routing problems in automated container terminals," *Comput. Ind. Eng.*, vol. 166, Apr. 2022, Art. no. 107968.

[3] S. Riazi, K. Bengtsson, and B. Lennartson, "Energy optimization of large-scale AGV systems," *IEEE Trans. Autom. Sci. Eng.*, vol. 18, no. 2, pp. 638–649, Apr. 2021, doi: 10.1109/TASE.2019.2963285.

[4] X. Dai, X. Li, Y. Li, and A. P. Hu, "Maximum efficiency tracking for wireless power transfer systems with dynamic coupling coefficient estimation," *IEEE Trans. Power Electron.*, vol. 33, no. 6, pp. 5005–5015, Jun. 2018, doi: 10.1109/TPEL.2017.2729083.

[5] N. Ali, Z. Liu, H. Armghan, and A. Armghan, "Double integral sliding mode controller for wirelessly charging of fuel cell-battery-super capacitor based hybrid electric vehicle," *J. Energy Storage*, vol. 51, Jul. 2022, Art. no. 104288.

[6] L. Sun, D. Ma, and H. Tang, "A review of recent trends in wireless power transfer technology and its applications in electric vehicle wireless charging," *Renew. Sustain. Energy Rev.*, vol. 91, pp. 490–503, Aug. 2018.

[7] A. Massa, G. Oliveri, F. Viani, and P. Rocca, "Array designs for long-distance wireless power transmission: State-of-the-art and innovative solutions," *Proc. IEEE*, vol. 101, no. 6, pp. 1464–1481, Jun. 2013.

[8] W. Zhou and K. Jin, "Efficiency evaluation of laser diode in different driving modes for wireless power transmission," *IEEE Trans. Power Electron.*, vol. 30, no. 11, pp. 6237–6244, Nov. 2015.

[9] R. Mai, B. Luo, Y. Chen, and Z. He, "Double-sided CL compensation topology based component voltage stress optimisation method for capacitive power transfer charging system," *IET Power Electron.*, vol. 11, no. 7, pp. 1153–1160, Jun. 2018.

[10] Y.-G. Su, W. Zhou, A. P. Hu, C.-S. Tang, S.-Y. Xie, and Y. Sun, "Full-duplex communication on the shared channel of a capacitively coupled power transfer system," *IEEE Trans. Power Electron.*, vol. 32, no. 4, pp. 3229–3239, Apr. 2017.

[11] D. Kim, A. Abu-Siada, and A. Sutinjo, "State-of-the-art literature review of WPT: Current limitations and solutions on IPT," *Electric Power Syst. Res.*, vol. 154, pp. 493–502, Jan. 2018.

[12] Y. Liu, K. Zhang, and A. P. Hu, "Investigation of reactive power distribution between two coils of inductive power transfer system by Poynting vector analysis," *Int. J. Electr. Power Energy Syst.*, vol. 136, Mar. 2022, Art. no. 107621.

[13] A. A. S. Mohamed, A. Berzoy, F. G. N. de Almeida, and O. Mohammed, "Modeling and assessment analysis of various compensation topologies in bidirectional IWPT system for EV applications," *IEEE Trans. Ind. Appl.*, vol. 53, no. 5, pp. 4973–4984, Sep. 2017, doi: 10.1109/TIA.2017.2700281.

[14] S.-J. Huang, T.-S. Lee, W.-H. Li, and R.-Y. Chen, "Modular on-road AGV wireless charging systems via interoperable power adjustment," *IEEE Trans. Ind. Electron.*, vol. 66, no. 8, pp. 5918–5928, Aug. 2019, doi: 10.1109/TIE.2018.2873165.

[15] C. Tan, Y. Chen, Y. Wu, Z. Xiao, and F. Dong, "A modular magnetic induction tomography system for low-conductivity medium imaging," *IEEE Trans. Instrum. Meas.*, vol. 70, pp. 1–8, 2021, doi: 10.1109/TIM.2021.3073439.

[16] R. Gao et al., "Small foreign metal objects detection in X-ray images of clothing products using faster R-CNN and feature pyramid network," *IEEE Trans. Instrum. Meas.*, vol. 70, pp. 1–11, 2021, doi: 10.1109/TIM.2021.3077666.

[17] K. Li, Y. Ren, Q. Gong, and Y. Li, "Magnetic excitation response optimization technique for detecting metal targets in middle-shallow strata," *IEEE Trans. Instrum. Meas.*, vol. 70, pp. 1–11, 2021, doi: 10.1109/TIM.2021.3123427.

[18] W. Zhang, Q. Mo, P. Yan, and Y. Liu, "Simultaneous metal object detection and coil alignment for wireless EV chargers using planar coil array," *IEEE Trans. Instrum. Meas.*, vol. 70, pp. 1–11, 2021, doi: 10.1109/TIM.2021.3126394.

[19] C. Liu, C. Jiang, and C. Qiu, "Overview of coil designs for wireless charging of electric vehicle," in *Proc. IEEE PELS Workshop Emerg. Technol., Wireless Power Transf. (WoW)*, May 2017, pp. 1–6, doi: 10.1109/WoW.2017.7959389.

[20] T. Fujita, T. Yasuda, and H. Akagi, "A dynamic wireless power transfer system applicable to a stationary system," *IEEE Trans. Ind. Appl.*, vol. 53, no. 4, pp. 3748–3757, Jul./Aug. 2017.

[21] P. K. Chittoor, B. Chokkalingam, and L. Mihet-Popa, "A review on UAV wireless charging: Fundamentals, applications, charging techniques and standards," *IEEE Access*, vol. 9, pp. 69235–69266, 2021, doi: 10.1109/ACCESS.2021.3077041.

[22] S. Pan, Y. Xu, Y. Lu, W. Liu, Y. Li, and R. Mai, "Design of compact magnetic coupler with low leakage EMF for AGV wireless power transfer system," *IEEE Trans. Ind. Appl.*, vol. 58, no. 1, pp. 1044–1052, Jan. 2022, doi: 10.1109/TIA.2021.3119906.

[23] S. Fukuda, H. Nakano, Y. Murayama, T. Murakami, O. Kozakai, and K. Fujimaki, "A novel metal detector using the quality factor of the secondary coil for wireless power transfer systems," in *IEEE MTT-S Int. Microw. Symp. Dig.*, May 2012, pp. 241–244.

[24] H. Jafari, M. Moghaddami, and A. I. Sarwat, "Foreign object detection in inductive charging systems based on primary side measurements," *IEEE Trans. Ind. Appl.*, vol. 55, no. 6, pp. 6466–6475, Nov./Dec. 2019, doi: 10.1109/TIA.2019.2937501.

[25] M. Singh and S. Bastami, "Apparatus, system, and method for detecting a foreign object in an inductive wireless power transfer system based on input power," U.S. Patent 9 553 485 B2, Jan. 24, 2017.

[26] K. D. Lee and Z. N. Low, "Systems and methods for detecting and identifying a wireless power device," U.S. Patent 9 252 846 B2, Feb. 2, 2016.

[27] M. Singh, "Apparatus, system, and method for detecting a foreign object in an inductive wireless power transfer system via coupling coefficient measurement," U.S. Patent 9 551 805 B2, Jan. 24, 2017.

[28] T. Sonnenberg, A. Stevens, A. Dayerizadeh, and S. Lukic, "Combined foreign object detection and live object protection in wireless power transfer systems via real-time thermal camera analysis," in *Proc. IEEE Appl. Power Electron. Conf. Expo. (APEC)*, Mar. 2019, pp. 1547–1552.

[29] X. Liu, C. Liu, W. Han, and P. W. T. Pong, "Design and implementation of a multi-purpose TMR sensor matrix for wireless electric vehicle charging," *IEEE Sensors J.*, vol. 19, no. 5, pp. 1683–1692, Mar. 2019, doi: 10.1109/JSEN.2018.2883708.

[30] Y. Lu and M. J. Higgins-Luthman, "Object detection and tracking system," U.S. Patent 8 027 029, Sep. 27, 2011.

[31] D. Bell and M. A. Leabman, "Systems and methods of object detection using one or more video cameras in wireless power charging systems," U.S. Patent 9 871 387 B1, Jan. 16, 2018.

[32] Y. Tian, W. Guan, G. Li, K. Mehran, J. Tian, and L. Xiang, "A review on foreign object detection for magnetic coupling-based electric vehicle wireless charging," *Green Energy Intell. Transp.*, vol. 1, no. 2, Sep. 2022, Art. no. 100007.

[33] Y. Zhang, Z. Yan, J. Zhu, S. Li, and C. Mi, "A review of foreign object detection (FOD) for inductive power transfer systems," *eTransportation*, vol. 1, Aug. 2019, Art. no. 100002.

[34] L. Xiang, Z. Zhu, J. Tian, and Y. Tian, "Foreign object detection in a wireless power transfer system using symmetrical coil sets," *IEEE Access*, vol. 7, pp. 44622–44631, 2019.

[35] S. Y. Jeong, V. X. Thai, J. H. Park, and C. T. Rim, "Self-inductance-based metal object detection with mistuned resonant circuits and nullifying induced voltage for wireless EV chargers," *IEEE Trans. Power Electron.*, vol. 34, no. 1, pp. 748–758, Jan. 2019.

[36] S. Y. Jeong, H. G. Kwak, G. C. Jang, S. Y. Choi, and C. T. Rim, "Dual-purpose nonoverlapping coil sets as metal object and vehicle position detections for wireless stationary EV chargers," *IEEE Trans. Power Electron.*, vol. 33, no. 9, pp. 7387–7397, Sep. 2018.

[37] A. Bharadwaj, A. Sharma, and C. C. Reddy, "An unconventional measurement technique to estimate power transfer efficiency in series–series resonant WPT system using S-parameters," *IEEE Trans. Instrum. Meas.*, vol. 71, pp. 1–9, 2022.

[38] K. Chen, Y. Ouyang, X. Yang, N. C. Cheung, E. K. W. Cheng, and J. Pan, "A high-interoperability optimal frequency control method for the AGV dynamic wireless charging systems without communication," *IEEE Trans. Power Electron.*, vol. 39, no. 3, pp. 3797–3808, Mar. 2024.

[39] J. Shin et al., "Design and implementation of shaped magnetic-resonance-based wireless power transfer system for roadway-powered moving electric vehicles," *IEEE Trans. Ind. Electron.*, vol. 61, no. 3, pp. 1179–1192, Mar. 2014.

[40] V. X. Thai, G. C. Jang, S. Y. Jeong, J. H. Park, Y. Kim, and C. T. Rim, "Symmetric sensing coil design for the blind-zone free metal object detection of a stationary wireless electric vehicles charger," *IEEE Trans. Power Electron.*, vol. 35, no. 4, pp. 3466–3477, Apr. 2020, doi: 10.1109/TPEL.2019.2936249.

[41] S. Y. Chu, X. Zan, and A.-T. Avestruz, "Electromagnetic model-based foreign object detection for wireless power transfer," *IEEE Trans. Power Electron.*, vol. 37, no. 1, pp. 100–113, Jan. 2022, doi: 10.1109/TPEL.2021.3100420.

[42] Y. Tian, Y. Lin, J. Tian, and L. Xiang, "Multi-thread sensing coil design for metal object detection of wireless power transfer systems," *Measurement*, vol. 184, Nov. 2021, Art. no. 109952.

Xiaodong Yang is currently pursuing the M.S. degree with the College of Mechatronics and Control Engineering, Shenzhen University, Shenzhen, China.

His research interests include the design and analysis of wireless power transfer technologies, dc–dc converter, and control theory.

Yuzhao Ouyang received the B.S. degree in rail transit signal and control from Linyi University, Linyi, China, in 2016, and the M.S. degree in electronic information from Shenzhen University, Shenzhen, China, in 2023.

His research interests include design and control of wireless power transfer systems.

Kaiwen Chen (Member, IEEE) was born in Zhejiang, China. He received the M.Sc. and Ph.D. degrees from Hong Kong Polytechnic University, Hong Kong, in 2017 and 2022, respectively.

His main research interests include wireless power transfer, electric vehicles, control theory, and artificial intelligence.

Norbert Cheung (Senior Member, IEEE) received the B.Sc. degree from the Queen Marry College, London University, London, U.K., in 1981, the M.Sc. degree from The University of Hong Kong, Hong Kong, in 1987, and the Ph.D. degree from the University of New South Wales, Sydney, NSW, Australia, in 1996.

He is currently with the College of Mechatronics and Control Engineering, Shenzhen University, Shenzhen, China. His research interests are actuators design, motion control, and robotics.

Jianfei Pan (Member, IEEE) received the Ph.D. degree from the Department of Electrical Engineering, The Hong Kong Polytechnic University, Hong Kong, in 2006.

He is currently with the College of Mechatronics and Control Engineering, Shenzhen University, Shenzhen, China. His main research interests include the design and control of linear motors and generators.